ACS APPLIED MATERIALS & INTERFACES

www.acsami.org Research Article

An Innovative Lithium Ion Battery System Based on a Cu_2S Anode Material

Yunhui Wang,[#] Xinran Feng,[#] Yin Xiong, Stanislav Stoupin, Rong Huang, Min Zhao, Mingsheng Xu, Peng Zhang,[*] Jinbao Zhao,[*] and Héctor D. Abruña[*]

Cite This: *ACS Appl. Mater. Interfaces* 2020, 12, 17396−17405 Read Online

ABSTRACT: Cu_2S is considered as one of the potential anode paradigms for advanced rechargeable batteries because of its high theoretical capacity (~335 $mAh \cdot g^{-1}$), high and flat charge/discharge voltage plateaus (~1.7 V vs Li^+/Li), stable cycling performance, and its elemental abundance. However, many studies have shown that Cu_2S exhibits a dramatic capacity fade in carbonate-based electrolytes, which has precluded its commercialization when paired with high voltage cathodes in state-of-the-art lithium ion batteries. Here, we report on a fundamental mechanistic study of the electrochemical processes of Cu_2S in both ether- and carbonate-based electrolytes employing *operando* synchrotron X-ray methods. Based on our findings, we developed a Cu_2S/C composite material that suppresses its failure mechanism in carbonate-based electrolytes and further demonstrated its feasibility in lithium ion full cells for the first time. Our experiment provides the basis for the utilization of Cu_2S in industrial-scale applications for large-scale electrical energy storage.

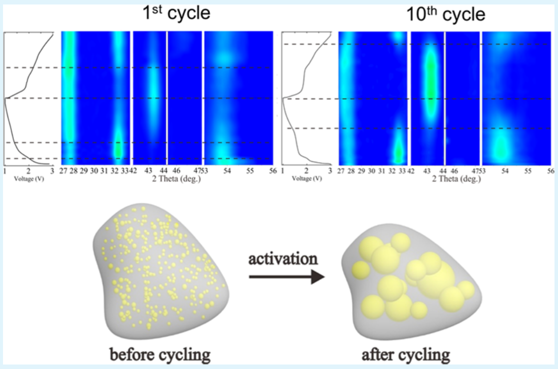

KEYWORDS: *Cu_2S, anode, electrolytes, lithium ion battery, synchrotron X-ray, X-ray absorption spectroscopy*

INTRODUCTION

Due to the increasing global awareness of the need for reducing fossil fuel reliance and greenhouse gas emissions in recent years, rechargeable batteries have emerged as one of the dominant energy storage technologies. Among them, lithium ion batteries (LIBs) have been the most successful in portable electronics and electric vehicles.[1] They surpass previous technologies in terms of cycle life and high energy/power densities, but concerns about their cost and safety remain, requiring alternative materials/systems to be developed.[2,3]

Copper-based sulfides (CuS and Cu_2S) are promising electrode materials for lithium ion batteries. They have gained a high level of interest due to their abundance, low cost, environmental friendliness, and excellent intrinsic functional properties, including its charge carrier mobility.[4,5] In a previous work, we showed that Cu_2S has better cycling and rate performance capabilities, arising from its higher conductivity and the displacement reaction between Cu_2S and Li_2S.[6]. Different from other conversion-reaction-based metal sulfides, Tarascon and Adelhelm et al. pointed out that copper sulfides exhibit a special displacement reaction, involving a process of highly reversible lithium/copper ions insertion/extrusion in the stable sulfur matrix based on the structural similarities between Cu_2S and its lithiated product (Li_2S) as well as the high mobility of Cu^+ within the Cu_2S lattice.[7−9] Upon discharge, micron-scale long Cu dendrites were observed, in which the Cu atoms were extruded out of the sulfur matrix. This unique mechanism could promote a stable cycling performance (in the hundreds of cycles without evident capacity fade) and excellent rate capability (up to 10 C).[10] Similar to $Li_4Ti_5O_{12}$, the high charge/discharge plateaus of Cu_2S (~1.7 V vs Li^+/Li) preclude the formation of hazardous lithium dendrites, making Cu_2S a particularly safe anode material. Relative to $Li_4Ti_5O_{12}$, Cu_2S has a much higher theoretical capacity (~335 $mAh \cdot g^{-1}$), which would yield a high energy density device when coupled to high voltage cathodes in state-of-the-art LIBs.[11] These properties have made Cu_2S attractive for designing advanced rechargeable batteries, especially for large-scale electrical energy storage applications. However, electrolyte matching remains to be a critical factor affecting the electrochemical behavior of Cu_2S and therefore has precluded its commercialization.[8] In essence, Cu_2S only exhibits stable cycling performance in ether-based electrolytes, which are not appropriate for high voltage cathodes owing to their limited electrochemical stability. On the other hand, carbonate-based electrolytes, which are

Received: December 4, 2019
Accepted: March 25, 2020
Published: March 25, 2020

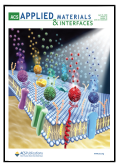

https://dx.doi.org/10.1021/acsami.9b21982
ACS Appl. Mater. Interfaces 2020, 12, 17396−17405

commonly used in commercial LIBs, are detrimental to Cu_2S, leading to a dramatic capacity fade in less than 10 cycles. Shi et al. investigated the failure mechanism of Cu_2S in carbonate-based electrolytes and found that the Cu_2S reacted with cyclic carbonates, in which the side reaction products deposited on the surface of the electrode, preventing it from further cycling.[12] Although Cu_2S electrodes could perform better in pure linear carbonates, the capacity of the Cu_2S cell continuously faded nevertheless. Moreover, it is impractical to only use the linear carbonates as solvents for lithium ion batteries. Cu_2S is often listed as a "promising" cathode material in numerous publications when paired with a lithium metal anode and cycled in ether-based electrolytes. This, however, remains far from practical due to the very challenging constraints of employing a lithium metal anode.[13−15]

It is thus crucial to understand the failure mechanism of Cu_2S in carbonate-based electrolytes and identify potential solutions. This could enable its commercialization as an anode in LIBs. In this manuscript, we present an investigation on the electrochemical responses of Cu_2S in both ether- and carbonate-based electrolytes under *operando* conditions, aiming to fundamentally understand their origins. *Operando* measurements enable the study of sensitive reaction intermediates, which is key to achieving a fundamental understanding of the real electrochemical processes under a battery's native environment.[16] We have developed a composite material, with a uniform carbon coating, capable of suppressing the surface reactions between Cu_2S and carbonate-based electrolytes to maintain its structural integrity and displacement mechanism, achieving stable electrochemical cycling performance in carbonate-based electrolytes. Furthermore, we assembled a full cell by coupling a Cu_2S/C composite as the anode with a $LiCoO_2$ cathode for the first time. This provided the basis for transferring Cu_2S to industrial-scale applications and battery systems for large-scale electrical energy storage.

EXPERIMENTAL SECTION

Materials. $CuSO_4·5H_2O$, $Na_2S_2O_3·5H_2O$, CuCl, CH_4N_2S (TA, thiourea), $(CH_2OH)_2$ (EG, ethylene glycol), and glucose were purchased from Sinopharm Chemical Reagent Corporation (analytically pure). CuO and Cu_2O (99+%; A.C.S. reagent) used as X-ray absorption spectroscopy standards were purchased from Aldrich Chemical Company, Inc. Cu_2S (99.5%) standard was from Alfa Aesar Chemicals.

Preparation of Cu_2S/C and Cu_2S. *Cu_2S/C.* $CuSO_4·5H_2O$ (0.005 mol), $Na_2S_2O_3·5H_2O$ (0.005 mol), and 1.2 g of glucose were sequentially added into deionized water (100 mL) with magnetic stirring for 20 min. The resulting mixture was spray-dried (Buchi mini-spray drier B-290) with nitrogen as the carrier gas. The inlet temperature and the rotameter settings were 200 °C and 40 mm, respectively. The aspirator and pump rates were 100 and 15%, respectively. The spray-dried precursors were transferred to a tube furnace and calcined for 8 h at 500 °C under the protection of Ar gas. The calcined products were washed with deionized water several times followed by vacuum drying overnight.

Cu_2S. A modified microwave (MW) method was used.[17] A 0.02 mol CuCl and 0.01 mol thiourea solution was added to 50 mL of EG and stirred for 20 min. The mixture was loaded into a microwave reactor (model: LWMC-201, microwave frequency: 2450 MHz, output power: 650 W) and radiated by a cyclic microwave treatment (18 s on, 42 s off) for 1 h. The resulting precipitate was washed in deionized water and absolute ethanol several times followed by drying in vacuum. The dried precursor was calcined at 350 °C for 6 h under an Ar atmosphere followed by cooling down to room temperature.

Physical Characterization. The morphologies of Cu_2S and the Cu_2S/C composites were characterized using scanning electron microscopy (SEM; Hitachi S-4800) and transmission electron microscopy (TEM; JEM-2100). Raman spectra (Renishaw plc., UK) were recorded using a laser wavelength of 532 nm excitation with a resolution of 1 cm^{-1}. Thermogravimetric analysis (TGA) was performed on an SDT Q600 (TA Instruments) analyzer, while TGA measurements were carried out under an air flow from room temperature to 800 °C at a heating rate of 10 °C min^{-1}.

Electrochemical Measurements. *Cu_2S/C Half Cells.* An electrode slurry was prepared by mixing the as-prepared Cu_2S/C (Cu_2S), acetylene black (AB), and polyvinylidene fluoride (PVDF) in a weight ratio of 7:1.5:1.5 and stirring with *N*-methyl-2-pyrrolidinone (NMP) for 3 h followed by coating onto a copper foil current collector with a doctor blade. The electrode was dried at 60 °C under vacuum for 24 h. CR2016-type coin cells were assembled in an Ar-filled glovebox with lithium metal as the counter electrode and Celgard 2400 as the separator. Two different types of electrolytes were used. The first was 1 M $LiPF_6$ dissolved in a 1:1 mixture of ethylene carbonate (EC) and diethyl carbonate (DEC). The other was 1 M lithium bis(trifluoromethanesulfonyl)imide (LiTFSI) dissolved in a 1:1 mixture of 1,3-dioxolane (DOL) and dimethyl ether (DME). Constant current and voltage (CC/CV protocol with a Neware battery program-control system) charge and constant current discharge measurements were performed at different current densities over the voltage range from 1.0 to 3.0 V versus Li^+/ Li at room temperature (the cell was charged at a constant current to 3.0 V then kept charging at 3.0 V until the current decreased to 1/10 of that constant current). Cyclic voltammetry tests were conducted on a CHI 1030C electrochemical workstation (Chenhua, Shanghai) at a scan rate of 0.2 mV s^{-1}. Electrochemical impedance spectra (EIS) over the frequency ranged from 10^{-1} to 10^5 Hz at different states of discharge/charge were conducted with a Metrohm Autolab PGSTAT 302N electrochemical workstation. Mass loadings of Cu_2S/C in the coin cells ranged from 1.2 to 1.5 mg cm^{-2}. The specific capacity of Cu_2S/C was calculated based on the total mass of the Cu_2S/C composite. All electrochemical measurements were conducted at room temperature.

$LiCoO_2/Cu_2S/C$ Pouch Cell. The positive (cathode) electrode consisted of single-sided 32 mm × 32 mm $LiCoO_2$-coated Al foil with a mass loading ($LiCoO_2$) of 3.1 mg cm^{-2} on one side of the foil (the weight ratio of $LiCoO_2$/AB/PVDF was 8:1:1). The Cu_2S/C (anode) electrode consisted of single-sided 30 mm × 30 mm Cu_2S/C-coated Cu foil with a mass loading of 1.5 mg cm^{-2} on one side of the foil. The pouch cell was assembled in a dried ambient environment followed by injection of the electrolyte (1 M $LiPF_6$ in EC/DEC) in an Ar-filled glovebox.

Operando Cells. The *operando* coin cells were made from CR2032-type coin cell casings. A 3 mm diameter hole was drilled in the center and sealed with Kapton polyimide film (0.13 mm-thick) using Torr Seal epoxy. A schematic diagram of the *operando* cell is shown in the Supporting Information (Figure S1). Aluminum foil was used as the current collector. *Operando* coin cells were cycled at 0.2 C with a Biologics SP-200 potentiostat.

***Operando* X-ray Absorption Spectroscopy Measurements.** Cu K-edge X-ray absorption spectroscopy (XAS) data collection was performed at beamline F-3 of the Cornell High Energy Synchrotron Source (CHESS). The measurements were done in transmission mode from 150 eV below the metal K-edge to 550 eV above the edge with N_2-filled ion chambers. A Cu metal foil spectrum was collected simultaneously to calibrate the incident X-ray energy and served as a reference spectrum. XANES (X-ray absorption near-edge structure) spectra were calibrated and normalized with the ATHENA software package. Fourier transformed EXAFS (extended X-ray absorption fine structure) spectra were obtained by applying a Hanning window from 3 to 11 $Å^{-1}$ with k^2-weighting in ATHENA and fitted with standard Cu_2S and Cu crystal structures using the ARTEMIS package.[18]

***Operando* X-ray Diffraction Measurements.** *Operando* powder X-ray diffraction (XRD) patterns were collected at beamline A-1 of the Cornell High Energy Synchrotron Source (CHESS) at an incident energy of 19.82 keV (λ = 0.6246 Å) using an ADSC Quantum-210 CCD detector. Dark current correction was applied to the collected 2D XRD patterns. A baseline diffraction pattern (snapshot) was

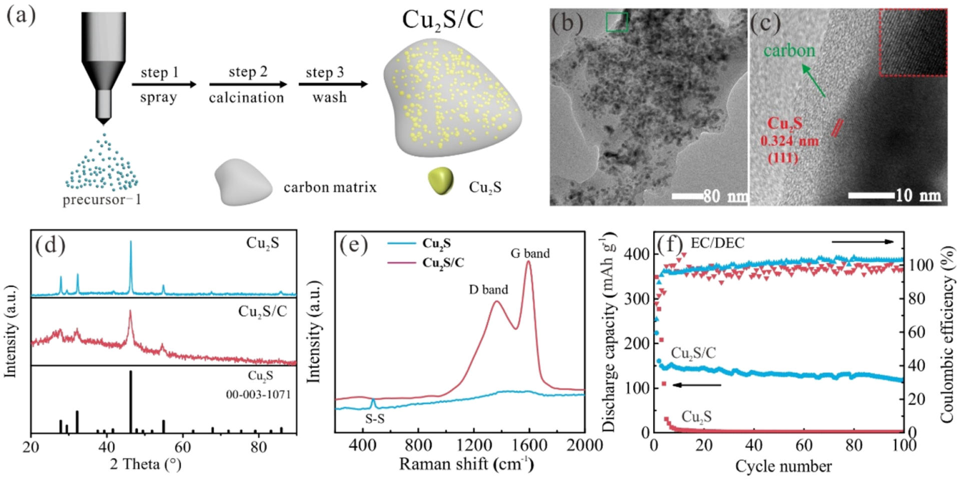

Figure 1. (a) Schematic illustration of the Cu_2S/C composite synthesis procedure. (b) TEM and (c) HR-TEM images of the Cu_2S/C composite (zoom-in image of Cu_2S lattice planes in the inset). (d) XRD patterns and (e) Raman spectra of Cu_2S and Cu_2S/C. (f) Cycling performances of Cu_2S and Cu_2S/C in EC/DEC at 200 mA g^{-1}. The specific capacity of Cu_2S/C was calculated based on the mass of the Cu_2S/C composite.

collected for an empty *operando* coin cell containing all parts, except for the Cu_2S/C electrode slurry to determine peaks from cell components and impurities. This background diffraction pattern was subtracted from the *operando* patterns during data analysis. The Kapton film and epoxy have minimal contributions to the diffracted signal. Each sample was exposed to the X-ray beam for 40 s every 4 min to minimize potential beam-induced damage. The obtained *operando* 2D XRD snapshots were reduced to 1D diffraction patterns by azimuthal integration using the GSAS-II software package.[19] To facilitate the interpretation of the resulting 1D XRD patterns, the radial coordinate (representing the modulus of the X-ray momentum transfer) was converted to the 2-theta scattering angle corresponding to the wavelength λ = 1.05406 Å of the commonly used Cu K_α X-ray source.

RESULTS AND DISCUSSION

Physical Properties and Electrochemical Performance of Cu_2S/C. To prevent the side reactions between Cu_2S and carbonate-based electrolytes, it is important to create a protection layer on the Cu_2S surface. Carbon coating, a common strategy for enhancing the performance of cathodes and anodes in LIBs, is an excellent choice due to its superior electrical conductivity, chemical/electrochemical stability, and mechanical strength. Considering the reactive sensitivity with carbonates and the volume change during cycling, an ordinary carbon coating strategy could not meet the requirements. Here, we employed an *in situ* carbon coating method to fabricate the Cu_2S/C composite. The synthesis procedure is illustrated in Figure 1a. A $CuSO_4$ and glucose aqueous dispersion was sprayed at 200 °C to obtain precursor-1. As the aqueous solution evaporated, while spraying at a high temperature, the concentration of precursor-1 gradually increased.[20] When sprayed at 200 °C, $S_2O_3^{2-}$ ions dissociate to SO_4^{2-} and HS^-. The latter reacts with Cu(II) ions to form cuprous sulfide and Na_2SO_4 as a byproduct, accompanied by the dehydration of glucose, which acted as the carbon source.[21] Precursor-1 was then transferred to a tube furnace and calcined at 500 °C under the protection of Ar gas to produce precursor-2, while the dehydrated glucose was carbonized into amorphous carbon. The byproducts were later removed by washing with H_2O, and the Cu_2S/C composite was obtained. Different from conventional synthetic methods, the *in situ* carbon coating method has the following advantages: (i) carbon coating and copper sulfides synthesis were completed simultaneously; (ii) nanoscale Cu_2S particles were obtained, which reduced the volume-change effects during cycling; and (iii) the Cu_2S nanoparticles were completely covered/protected by the carbon layer, preventing their contact with the carbonate-based electrolytes.

The morphology and structure of the Cu_2S/C composite and Cu_2S were confirmed by TEM and XRD. The TEM image of the Cu_2S/C composite (Figure 1b) showed that the Cu_2S nanoparticles, which have a higher contrast in the image, were embedded in the carbon matrix with an amorphous structure. The lattice spacing of 0.324 nm was indexed to the (111) plane of Cu_2S (Figure 1c). The XRD patterns (Figure 1d) of Cu_2S and Cu_2S/C are well indexed to the standard card of Cu_2S (JCPDS: 003-1071). The high background signal and broad peak width of the Cu_2S/C XRD pattern were attributed to the amorphous carbon and small Cu_2S particle size in the composite, respectively. The prepared Cu_2S had a flake morphology with a thickness of about 50 nm (Figure S2a,b). The HRTEM image (Figure S2d) confirmed the lattice spacing of 0.278 nm, which is ascribed to the (200) planes of Cu_2S. Raman spectroscopy measurements were performed for Cu_2S and Cu_2S/C. In Figure 1e, the peaks at 1360 and 1594 cm^{-1} correspond, respectively, to the D and G bands of the carbon matrix.[22,23] The typical S−S peak at near ~470 cm^{-1} was observed for Cu_2S, but not for Cu_2S/C. This may be related to the strong light absorbing ability of the wrapping carbon matrix.[24,25] Figure S3 shows the TGA weight loss profile of Cu_2S/C. At temperatures above 700 °C, Cu_2S was oxidized to Cu_2O, and the carbon was completely consumed.[13] The carbon content was calculated to be 39.9 wt % (the detailed calculation is shown in Figure S3).

As previously reported, the choice of electrolyte is the determining factor for the cycling performance of Cu_2S. Jache et al. have shown that Cu_2S exhibits excellent cycling performance in an ether-based electrolyte (DOL/DME), whereas it failed within several cycles in a carbonate-based electrolyte (EC/DEC).[8] Our study further demonstrated that the cyclic carbonate electrolyte (EC) was disastrous to the cycling performance of Cu_2S in a way that was similar to the incompatibility between carbonate-based electrolytes and Li−S batteries.[12,26,27] Cu_2S/C composites overcame this limitation

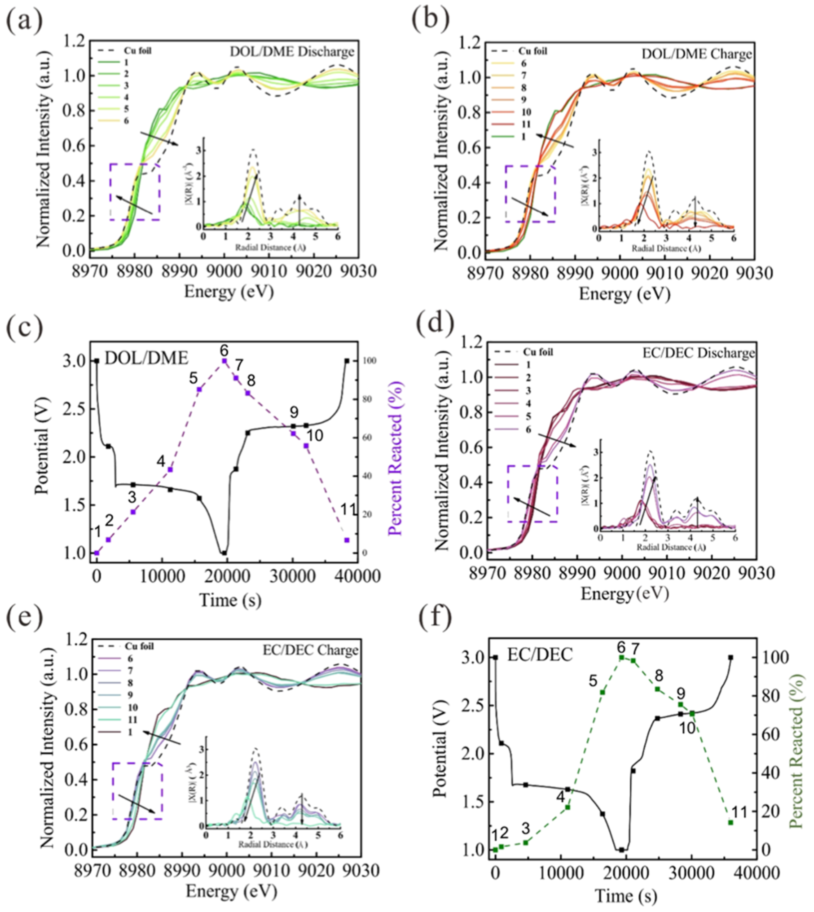

Figure 2. XANES patterns of Cu_2S in (a, b) DOL/DME and (d, e) EC/DEC electrolytes. The insets are the corresponding EXAFS patterns. Corresponding (dis)charge profiles and percentages of reacted Cu_2S in (c) DOL/DME and (f) EC/DEC.

by not only surviving in carbonate-based EC/DEC electrolytes but also achieving stable reversibility and cycling. It achieved a reversible capacity of 123 mAh g^{-1} (corresponding to a capacity of 192 mAh g^{-1} based on the mass of Cu_2S) after 100 cycles, while the capacity of the unprotected Cu_2S quickly decayed to 0 within 10 cycles (Figure 1f). Since the key point of this work is to provide a strategy to address the issue of incompatibility between Cu_2S and carbonate-based electrolytes, the carbon content was not optimized. The capacity of Cu_2S/C can be further improved by reducing the carbon content on the premise that the protection layer is still effective. The increase in Coulombic efficiency during the extended cycling may be artificially caused by parasitic reactions. The cycling performances of Cu_2S and Cu_2S/C in the DOL/DME electrolyte were also tested (Figure S4). Agreeing with previous reports, both exhibited excellent cycling stabilities.[6,8,10] After 100 cycles, the discharge capacities of Cu_2S and Cu_2S/C were 333 and 250 mAh g^{-1} (based on the mass of the Cu_2S/C composite), respectively. It has been reported that the excellent cycling performance of Cu_2S can be ascribed to its unique displacement reaction. The sulfur ions can be considered as an array (sulfur array/framework), in which both Cu(I) and Li(I) ions, with similar ionic radii, can insert/extrude reciprocally during charge and discharge processes, thus maintaining the structural integrity of the sulfur array.[7−9] The 2.1 V discharge plateau is related to the lithiation of nonstoichiometric cuprous sulfide, which will be explained in the Evolution in Crystal Structure in DOL/DEM and EC/DEC Electrolytes section below. The charge plateau at 2.3 V (which decays on subsequent cycles) of Cu_2S (Figure S5a,b) was ascribed to the electrochemical reactions associated with Li_2S, which were also observed in a previous work.[8] Upon subsequent cycling, a pair of flat (dis)charge plateaus at 1.8 V emerged (Figure S5a,c), which are ascribed to the highly reversible reaction between Cu_2S and Cu/Li_2S.[8,28,29] On the other hand, in EC/DEC electrolytes, Cu_2S exhibits poor cycling performance. The (dis)charge profiles decay after 5 cycles, while those of Cu_2S/C can be clearly observed after 100 cycles (Figure S5d). Furthermore, the long-term cycling performance of Cu_2S/C was tested at 20 mA g^{-1}. After 200 cycles, a reversible capacity of 118 mAh g^{-1} was obtained (corresponding to a capacity of 197 mAh g^{-1} based on the mass of Cu_2S) (Figure S6). The improved cycling performance is closely related to the carbon matrix protection of the Cu_2S active material, which also suggests the possibility of making carbonate-based electrolytes compatible with Cu_2S.

Operando XAS Investigation of the Cu_2S Mechanism in Ether/Carbonate-Based Electrolytes. Intrigued by the behavioral difference of Cu_2S in carbonate- and ether-based electrolytes, *operando* X-ray absorption spectroscopy (XAS) measurements were performed for Cu_2S in the two above-mentioned electrolytes. The XAS spectra for powder samples (Cu_2S synthesized via the microwave (MW) method, Cu_2S/C, commercial Cu_2S, and Cu_2O) are shown in Figure S7. The very similar spectral shapes of the synthesized Cu_2S and the commercial Cu_2S (c-Cu_2S) and Cu_2O (c-Cu_2O) samples

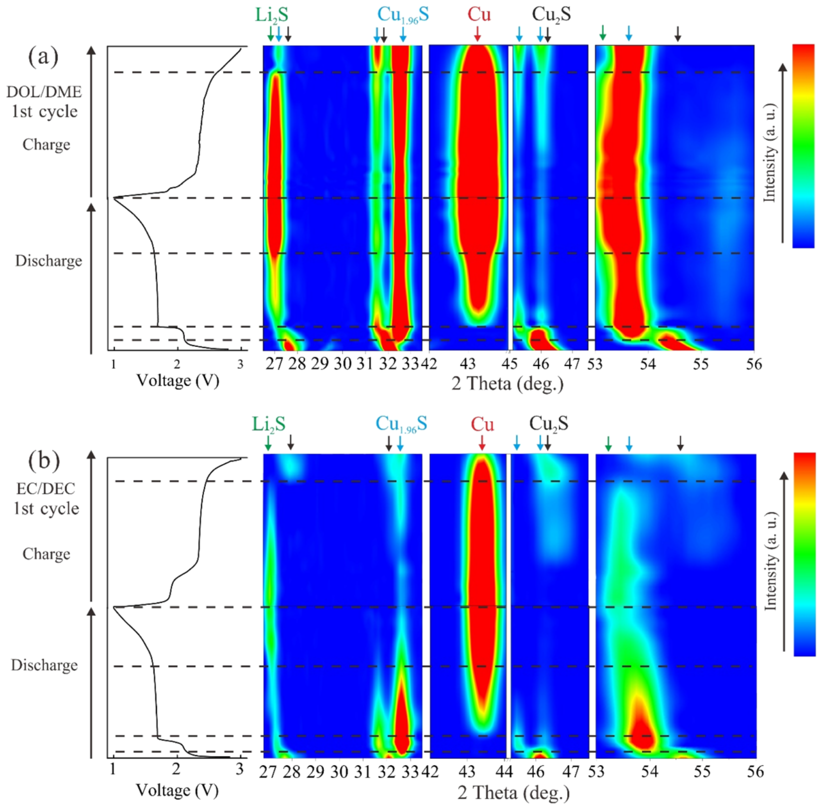

Figure 3. *Operando* XRD measurements and corresponding initial (dis)charge curves of Cu_2S (a) in DOL/DME and (b) EC/DEC electrolytes with 1 M LiPF6 at 0.2 C.

demonstrated that Cu_2S and Cu_2S/C had been successfully synthesized. This is also in accordance with the XRD and TEM data shown previously. The Cu valence states of synthesized Cu_2S (Cu_2S and Cu_2S/C) were first analyzed, with c-Cu_2S and c-Cu_2O used as standards. The edge energies of c-Cu_2S and c-Cu_2O were 8979.98 and 8980.26 eV, respectively. The slightly lower edge energy of c-Cu_2S resulted from the higher covalency between Cu−S bonds when compared to Cu−O bonds. The edge energy of the Cu_2S/C (8980.13 eV) was close to those of c-Cu_2S and c-Cu_2O, indicating a +1 oxidation state of Cu in Cu_2S/C. However, the synthesized Cu_2S exhibited a higher edge energy of 8981.21 eV, suggesting a higher oxidation state of Cu compared with the others. This could come from a small amount of Cu_2S readily oxidized in air, leading to the emergence of nonstoichiometric cuprous sulfide. Such a trace amount of nonstoichiometric cuprous sulfide could also explain the presence of a discharge voltage plateau at 2.1 V (Figure S5b).[17,30] Moreover, the edge energy differences between Cu_2S and Cu_2S/C also indicate that the carbon wrapping serves as a protective layer and prevents the oxidation of Cu.[31]

The *operando* XAS spectra of Cu_2S and their corresponding voltage/time profiles are presented in Figure 2a−c and d−f, for experiments in DOL/DME and EC/DEC electrolytes, respectively. As shown in Figure 2a,d, Cu_2S experiences a similar transition during the discharge process in both electrolytes, where it is gradually reduced to elemental copper. This was evident from a comparison of the edge energy at the end of the discharge (pt. 6) with that of the Cu foil as well as the similar oscillations above the white line. The isosbestic points in the spectra are consistent with a single redox reaction of Cu_2S during the electrochemical processes without any interference or side reactions.[32] Comparing the fully discharged XANES spectra (pt. 6) in both electrolyte systems with the Cu foil spectrum, the edge feature and the overall oscillations of the *operando* spectra exhibit a more smeared appearance. This is likely due to the smaller size of the metallic copper formed during the discharge process compared with the bulk, which was previously shown by both experimental methods and multiple scattering calculations.[33−35] The transition from Cu_2S to Cu can also be observed through the EXAFS spectra (inset). The peaks in the spectra reflect the bond distances between Cu and its surrounding S and Cu. In all inset EXAFS figures, the peak at around 1.9 Å in the pristine (initial) or fully recharged state represents the Cu−S bond distance in Cu_2S, while the peaks at 2.2 Å, in the fully discharge state (pt. 6), represent the Cu−Cu bonds. The three connected humps from 3 to 5.5 Å in the fully discharged scan are from both single and multiple electron scatterings between the center Cu and the second and third shell Cu atoms. The clear appearance of outer shell peaks is a strong evidence as to the formation of Cu clusters. The peak fitting results are presented in the Supporting Information (Figure S8). Different from the XANES spectra, EXAFS changes show that, in the DOL/DME electrolyte, the sulfur atoms change in a gradual manner, in contrast to the more sudden/abrupt transition from Cu−S to Cu−Cu in EC/DEC. Moreover, the EXAFS spectra also confirm the formation of copper clusters from the emergence of the first coordination Cu−Cu shell at 2.1 Å as well as the second and third copper shell multiple scatterings from 3 to 5.5 Å before phase correction. As for the charging process, Cu(0) is reoxidized to Cu(I) in both electrolytes during which the Cu is oxidized slowly at the beginning of the charge process and rapidly shifts to the Cu_2S

edge energy at the end of the charge (Figure 2b,e). However, after closely comparing the spectra, it is observed that at the end of charge (pt. 11), the rising edge energy in DOL/DME is closer to the pristine scan (pt. 1), compared with the one in the EC/DEC system (highlighted in the purple dashed line box). This suggests a more reversible chemical reaction in the ether-based electrolyte. Similarly, the EXAFS spectra for the charging process show larger differences between the two electrolyte systems. In DOL/DME, the Cu−S bonds gradually reform by slowly consuming the Cu clusters, according to the shift in the first Cu−Cu shell to Cu−S and the disappearance of Cu−Cu scattering from the second/third shells at 3−5.5 Å. In EC/DEC, it is apparent that the Cu atoms prefer to stay in the form of Cu clusters through most of the charging process and only switch to Cu_2S at the end of the recharge. This is supported by the EXAFS spectra that, except for the last scan (pt. 11), largely resemble the one at the end of discharge (pt. 6). The decrease in peak intensity can be explained by the loss in Cu_2S crystallinity as the Li_2S/Cu is converted to Cu_2S.

The amount of reacted Cu_2S throughout the entire cycle can be calculated using linear combination analysis. The pristine (initial) spectrum (scan 1) and the most discharged spectrum (scan 6) were used as references. The results are plotted in Figure 2c,f. Comparing these two figures, it is evident that Cu_2S, in the carbonate electrolyte, was oxidized more slowly during the charging process. This may arise from the fact that the diffused sulfide species formed byproducts with carbonate-based electrolyte during discharge, making it harder for Cu to recapture sulfur ions during the charge process.[26] In addition, in EC/DEC, most Cu atoms prefer to remain as Cu(0) through the charge process, indicating that there is a higher reaction barrier for the reformation of Cu_2S, in accordance with the larger overpotentials in EC/DEC. TEM analysis of Cu_2S electrodes after 10 cycles in both electrolytes was carried out (Figure S9). Compared to the pristine Cu_2S with fine crystallinity (Figure 1b,c), cycled Cu_2S in both electrolytes turned polycrystalline. In DOL/DME, $Cu_{1.96}S$ (the reason for choosing this phase will be articulated in the next section), which has a highly similar crystalline structure to that of Li_2S, has a lattice spacing of 0.327 nm, which can be ascribed to the (102) face of $Cu_{1.96}S$.[5] On the other hand, the crystalline orientation of products in EC/DEC is disordered, though the lattices ascribed to Cu and $Cu_{1.96}S$ can still be observed. Based on the results discussed above, the performance of Cu_2S in carbonate-based electrolytes is inferior, relative to ether electrolytes, for the following reasons: (i) the abruptness of the crystal structure transition is detrimental to maintaining the sulfur backbone structure; (ii) the higher energy barrier of the Cu_2S reformation results in a higher overpotential; and (iii) sulfide species dissolution is severe due to side reactions with carbonate-based electrolytes, resulting in significant sulfur loss.[26,27]

Evolution in Crystal Structure of Cu_2S in DOL/DEM and EC/DEC Electrolytes. Figure 3 presents the *operando* XRD evolution of the Cu_2S crystal structure during the 1st cycle in DOL/DME and EC/DEC electrolytes, respectively. In the case of DOL/DME (Figure 3a and Figure S11a), the diffraction peaks (27.7, 32.1, 46.2, and 54.9°) of pristine Cu_2S shift to lower angles followed by the emergence of a new phase. The small peak shifts (∼2.1 V) are attributed to the lattice expansion resulting from the lithiation of nonstoichiometric cuprous sulfide. The diffraction peaks of the new phase are well indexed to the standard pattern of tetragonal $Cu_{1.96}S$ (PDF 00-012-0224) (Figure S10), which is the electrochemically active intermediate reported by others.[36−38] To further verify the presence of $Cu_{1.96}S$, a Rietveld refinement analysis was performed on the fully charged Cu_2S in the DOL/DME electrolyte. The result is shown in Figure S12 and confirms that $Cu_{1.96}S$ is the final product in the DOL/DME electrolyte. The peaks associated with the Al current collector and Cu residual are labeled with stars, and align well with the peaks in the residual error. Previous reports have stated that the valence state of Cu in $Cu_{1.96}S$ is +1.[39,40] This statement was corroborated by XPS measurement of Cu 2p and S 2p binding energies. In fact, the valence state of Cu was +1 in all Cu_xS when $1.8\leq x \leq 2$. The difference in the Cu/S ratio between $Cu_{1.96}S$ and Cu_2S is due to their crystal structures: $Cu_{1.96}S$ has 8 [$Cu_{31}S_{16}$] in one-unit cell and Cu_2S has 48 [Cu_2S]. Thus, even though $Cu_{1.96}S$ was formed in the DOL/DME electrolyte, the reaction mechanism proposed here is charge and mass balanced. The Cu signal at 43.2° is detected at the beginning of the 1.7 V discharge plateau, and those of Li_2S (27 and 53.1°) are observed in the second half of the 1.7 V flat plateau, indicating the displacement reaction of $Cu_{1.96}S$. During the charge process, the reverse reaction takes place, judging from the signals of Cu and Li_2S. It is interesting to note that at the fully charged state, the tetragonal $Cu_{1.96}S$ phase is regenerated instead of the pristine cubic Cu_2S phase. After 10 cycles, the electrochemical reactions between $Cu_{1.96}S$ and Li_2S/Cu take place reversibly (Figure S13).

During the initial discharge process in EC/DEC (Figure 3b and Figure S11b), the Cu_2S experiences a similar discharge as with DOL/DME, with the peak shifts and phase transformation to $Cu_{1.96}S$ as discussed above. Nevertheless, when the battery was recharged to 2.5 V, not only is the $Cu_{1.96}S$ observed but also the cubic phase Cu_2S, which is different from the behavior in DOL/DME. The weaker signals indicate a smaller amount of regenerated Cu_2S. In the 2nd cycle (Figure S14), the transformation from cubic Cu_2S to tetragonal $Cu_{1.96}S$ continues followed by reduction to Li_2S and Cu. In the fully recharged state, Cu_2S is again regenerated. This could result from side reactions of sulfide with the carbonate-based electrolyte, which reduces the amount of sulfur participating in the recharge process. The XRD pattern of the Cu_2S electrode from the fully charged "dead" cell (after 10 cycles, charged to 3 V, ED/DEC electrolyte) (Figure S15) exhibited the presence of Li_2S, Cu, and $Cu_{1.96}S$. Cu_2S peaks are missing in the pattern, which is ascribed to the higher energy barrier of the Cu_2S reformation processes in EC/DEC. Thus, with subsequent cycling, the amount of Cu_2S regenerated continuously reduced. Though Li_2S, Cu, and $Cu_{1.96}S$ are electrochemically active, the cell cannot deliver any reversible capacity. In a previous publication, we studied the reactions of Cu_2S with carbonate-based electrolytes.[21,22] In the case of Cu_2S, the Cu_2S electrode from a "dead" cell could still deliver some capacity after being rinsed with dimethyl sulfoxide (DMSO). This indicated that the activity of Cu_2S was hindered by the presence of side products on the surface, which was also shown by X-ray photoelectron spectroscopy (XPS) results.

To analyze the surface conditions of the Cu_2S electrode, *in situ* EIS tests were carried out. In DOL/DME (Figure S16), the EIS profile is divided into two parts during discharge (Figure S16a−c). At the 2.1 V discharge plateau, the higher impedance is related to the lithiation process. The 1.7 V discharge plateau exhibits a smaller impedance, coinciding with

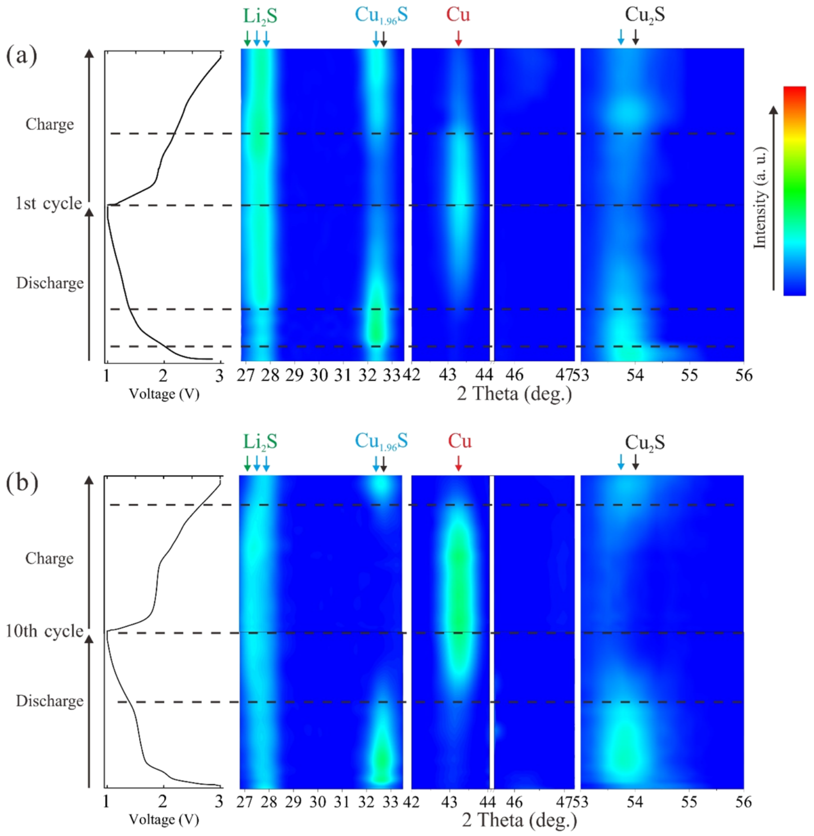

Figure 4. *Operando* XRD measurements and corresponding (dis)charge curves of Cu_2S/C in the (a) 1st cycle and (b) 10th cycle in EC/DEC electrolytes with 1 M $LiPF_6$.

the displacement reaction of the tetragonal $Cu_{1.96}S$. During the recharge process, the impedance increases slightly. After 10 cycles (Figure S16d−f), although the impedance increases at certain stages, the 1.7 V plateau still exhibits a smaller impedance. When the cell is fully recharged, the spectrum recovered to that at the OCV in the 10th cycle. In EC/DEC (Figure S17), the spectra are dramatically different. The 2.1 V discharge plateau shows a lower impedance, while the impedances at 1.7 V discharge plateau increase. When the cell is fully charged, the impedance is clearly larger, and after 10 cycles, it is extremely large. Based on the EIS results, we calculated the apparent lithium ions diffusion coefficients (Table S2).[41−43] For Cu_2S, the diffusion coefficient barely changed in DOL/DME after 10 cycles, while it experienced a 10^4-fold decrease in EC/DEC under otherwise identical conditions. These results also explain the failure of the cell. Based on previous and present results, it can be concluded that both side reactions and reaction pathways dramatically affect the reversibility of Cu_2S in ether- and carbonate-based electrolytes. In EC/DEC, Li_2S and Cu follow a more difficult reaction pathway to reform the cubic Cu_2S. Thus, it is difficult to maintain the sulfur array, leading to a loss in capacity. The side (decomposition) products cover the surface of the electrode, preventing further reaction. In DOL/DME, the structural similarity between the tetragonal $Cu_{1.96}S$ and Li_2S ensures an excellent reaction reversibility.

Structural Evolution and Activation Processes of Cu_2S/C in EC/DEC Electrolyte. Figure 4 and Figure S18 show the structural evolution of Cu_2S/C in the 1st and 10th cycles, respectively, in EC/DEC. During the initial discharge process, the peak at 32.1° intensifies. As discussed before, this peak is related to the emergence of the tetragonal phase $Cu_{1.96}S$. During continuous discharge, the peaks at 27.1 and 43.3° ascribed to Li_2S and Cu, respectively, indicating the displacement reaction ($Cu_{1.96}S + Li \rightarrow Cu + Li_2S$). During the initial charge process, the peaks associated with Cu and Li_2S lose intensity, while the peaks ascribed to $Cu_{1.96}S$ intensify. However, closer inspection of the XRD profile indicated that not all $Cu_{1.96}S$ reacted in the first cycle, as suggested by the residual peak at 32.1° and the minimal peak shift at 43.3°. This may indicate that, in addition to the redox reaction of Cu_2S, side reactions, such as the lithiation of carbon, may also contribute to the capacity of the battery. This observation coincides with the slanted (dis)charge plateaus and the *operando* XAS spectra (Figure S19), which suggest an incomplete reduction of Cu and are consistent with the apparent absence of isosbestic points. After 10 cycles (Figure 4b), the increase in intensity of the peak at 43.2° indicates the activation of Cu_2S/C, which can also be observed from the TEM images (Figure S20). When the cell is fully recharged, the emergence of peaks indexed to $Cu_{1.96}S$ demonstrates the reversible reaction of Cu/Li_2S to $Cu_{1.96}S$. The behavior of Cu_2S/C in EC/DEC is similar to that of Cu_2S in DOL/DME electrolytes. Additionally, the peak at 32.1°, associated with $Cu_{1.96}S$, disappears during discharge and remerges at the end of the recharge, indicating the complete reaction of the active material at the 10th cycle. This, together with the more defined voltage plateaus and CV profiles (Figure S21), demonstrates that $Cu_{1.96}S$ is the sole active material that contributes to the battery capacity; hence, the activation process of Cu_2S/C is demonstrated. *Operando* XRD indicated that the amorphous carbon wrapping successfully hindered the structural decom-

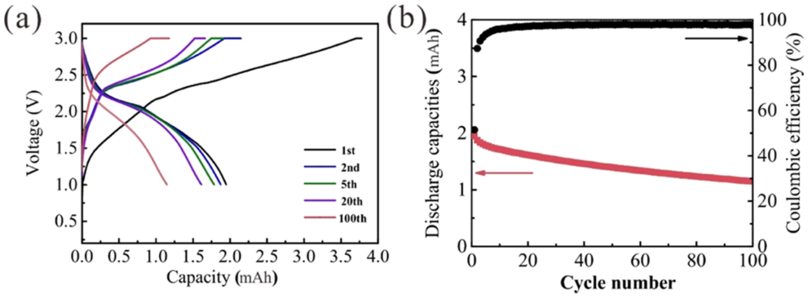

Figure 5. (a) Charge and discharge profiles and (b) cycling performance of the $LiCoO_2$-Cu_2S/C full cell at 100 mA g^{-1} (the capacity was calculated based on the mass of Cu_2S).

position and the loss of active material in EC/DEC electrolytes.

In situ EIS measurements were also performed on Cu_2S/C. In DOL/DME (Figure S22), the variation in the 1st cycle was similar to that in Cu_2S in DOL/DME (Figure S16). After 10 cycles, the impedance decreased, in accordance with the activation process observed. It is noted that, in EC/DEC (Figure S23), the change in the impedance in the 1st cycle was also similar to the stable impedance changes in DOL/DME (Figure S22). At the fully charged stage, a dramatic increase in impedance, similar to the case of Cu_2S in EC/DEC (Figure S17), was not observed. After 10 cycles, only minimal changes were noted in the EIS spectra suggesting a stable surface for the Cu_2S/C electrode, validating the effectiveness of the carbon coating. The lithium ion diffusion coefficient was also determined for the Cu_2S/C composite showing an only 6-fold decrease in EC/DEC after 10 cycles, when compared with the 10^4-fold drop for Cu_2S without carbon protection (Table S2). The results again demonstrate the compatibility between Cu_2S/C and EC/DEC electrolytes, in which the carbon matrix effectively hinders the surface reactions and helps retain the same reversible reaction pathways exhibited in DOL/DME electrolytes.

Electrochemical Performance of a (−) Cu_2S/C|1 M $LiPF_6$ in EC/DEC|$LiCoO_2$ (+) Pouch Cell. The *in operando* X-ray analysis provided a detailed understanding of the differences in the electrochemical performance of Cu_2S in ether- and carbonate-based electrolytes. It not only provided a deeper and more fundamental understanding of the electrochemical behavior but also provided insights for solving the mismatch between the Cu_2S and carbonate electrolytes, moving a step forward toward a practical battery system. The strategy of forming Cu_2S/C composite materials effectively hindered the loss of structural integrity and the side reactions between Cu_2S and carbonate-based electrolytes and thus maintained the highly reversible displacement reaction mechanism, which yielded excellent cycling performance. To further illustrate the viability of Cu_2S/C composites in practical use, $LiCoO_2$-Cu_2S/C pouch full cells were assembled with EC/DEC as the electrolyte (Figure 5). To the best of our knowledge, this is the first time that a full cell has been made by coupling Cu_2S as the anode with a commercial $LiCoO_2$ cathode. This provided the basis for the transfer, to industrial-scale applications, of this type of material and battery systems. The initial charge capacity and initial Coulombic efficiency (CE) were 3.79 mAh and 51%, respectively. The low initial CE is related to the properties of the amorphous carbon in Cu_2S/C, which can also be seen in the CE of Cu_2S/C in half cells being only 68% (Figure 1f). The CE then quickly increased in the initial cycles and eventually stabilized at over 98%. The discharge capacities in the 2nd and 20th cycles were 1.87 and 1.61 mAh, respectively. After 100 cycles, a reversible capacity of 1.15 mAh was achieved, accompanied by a decay rate of 0.68% per cycle. Although the performance of the full cell needs to be further optimized, these preliminary results have opened up a promising direction for a new lithium ion battery system exhibiting low cost and good cyclability with high energy density for large-scale energy storage and sustainable energy conversion.

CONCLUSIONS

By employing *in operando* synchrotron XRD and XAS techniques, the electrochemical reactions of Cu_2S in EC/DEC were found to be more irreversible than in an ether-based electrolyte system (DOL/DME). This critical problem could be solved by an *in situ* carbon coating approach, in which a carbon matrix effectively hinders the deleterious surface reactions and helps in retaining the same reaction pathways in DOL/DME. These key findings provide deep insights into the different behaviors in different electrolyte systems and make the cuprous sulfide, or even other metal sulfides, potentially viable for commercial lithium ion batteries. Based on these findings, we have, for the first time, successfully coupled a Cu_2S/C composite anode with a $LiCoO_2$ cathode in a commercial carbonate-based electrolyte system (EC/DEC).

ASSOCIATED CONTENT

Supporting Information

The Supporting Information is available free of charge at https://pubs.acs.org/doi/10.1021/acsami.9b21982.

Additional physical characterizations of the Cu_2S and Cu_2S/C (SEM, TEM, TGA, XRD, and XAS) and additional electrochemical tests (cycling profile, CV, and EIS) (PDF)

AUTHOR INFORMATION

Corresponding Authors

Peng Zhang − *College of Chemistry and Chemical Engineering, College of Energy, State Key Lab of Physical Chemistry of Solid Surfaces, Collaborative Innovation Center of Chemistry for Energy Materials, State-Province Joint Engineering Laboratory of Power Source Technology for New Energy Vehicle, Engineering Research Center of Electrochemical Technology (Ministry of Education), Xiamen University, Xiamen, Fujian 361005, China; Department of Chemistry and Chemical Biology, Baker Laboratory, Cornell University, Ithaca, New York 14853, United States*; Email: pengzhang@xmu.edu.cn

Jinbao Zhao − *College of Chemistry and Chemical Engineering, College of Energy, State Key Lab of Physical Chemistry of Solid Surfaces, Collaborative Innovation Center of Chemistry for Energy Materials, State-Province Joint Engineering Laboratory of Power Source Technology for New Energy Vehicle, Engineering Research Center of Electrochemical Technology (Ministry of Education), Xiamen University, Xiamen, Fujian 361005, China;* orcid.org/0000-0002-2753-7508; Email: jbzhao@xmu.edu.cn

Héctor D. Abruña − *Department of Chemistry and Chemical Biology, Baker Laboratory, Cornell University, Ithaca, New York 14853, United States;* orcid.org/0000-0002-3948-356X; Email: hda1@cornell.edu

Authors

Yunhui Wang − *College of Chemistry and Chemical Engineering, College of Energy, State Key Lab of Physical Chemistry of Solid Surfaces, Collaborative Innovation Center of Chemistry for Energy Materials, State-Province Joint Engineering Laboratory of Power Source Technology for New Energy Vehicle, Engineering Research Center of Electrochemical Technology (Ministry of Education), Xiamen University, Xiamen, Fujian 361005, China*

Xinran Feng − *Department of Chemistry and Chemical Biology, Baker Laboratory and Cornell High Energy Synchrotron Source (CHESS), Cornell University, Ithaca, New York 14853, United States*

Yin Xiong − *Department of Chemistry and Chemical Biology, Baker Laboratory, Cornell University, Ithaca, New York 14853, United States*

Stanislav Stoupin − *Cornell High Energy Synchrotron Source (CHESS), Cornell University, Ithaca, New York 14853, United States*

Rong Huang − *Cornell High Energy Synchrotron Source (CHESS), Cornell University, Ithaca, New York 14853, United States*

Min Zhao − *College of Chemistry and Chemical Engineering, College of Energy, State Key Lab of Physical Chemistry of Solid Surfaces, Collaborative Innovation Center of Chemistry for Energy Materials, State-Province Joint Engineering Laboratory of Power Source Technology for New Energy Vehicle, Engineering Research Center of Electrochemical Technology (Ministry of Education), Xiamen University, Xiamen, Fujian 361005, China*

Mingsheng Xu − *College of Chemistry and Chemical Engineering, College of Energy, State Key Lab of Physical Chemistry of Solid Surfaces, Collaborative Innovation Center of Chemistry for Energy Materials, State-Province Joint Engineering Laboratory of Power Source Technology for New Energy Vehicle, Engineering Research Center of Electrochemical Technology (Ministry of Education), Xiamen University, Xiamen, Fujian 361005, China*

Complete contact information is available at:
https://pubs.acs.org/10.1021/acsami.9b21982

Author Contributions

[#]Y.W. and X.F. contributed equally to this work.

Author Contributions

P.Z., J.Z., and H.D.A. conceived the idea. Y.W. synthesized the materials and conducted the electrochemical study. X.F. performed the *operando* synchrotron measurements. Y.X., M.Z., and M.X. helped perform the experiment. S.S. and R.H. set up the synchrotron instruments. Y.W., X.F., P.Z., and H.D.A. contributed to writing the paper. All the authors participated in the analysis of the experimental data and discussions of the results as well as preparing the paper.

Notes

The authors declare no competing financial interest.

■ ACKNOWLEDGMENTS

This work is financially supported by the National Natural Science Foundation of China (grant nos. 21621091 and 21875195) and the National Key Research and Development Program of China (2017YFB0102000) and is also based upon the research conducted at the Cornell High Energy Synchrotron Source (CHESS), which is supported by the National Science Foundation under award DMR-1332208. Y.W. sincerely thanks Prof. Daiwei Liao for his valuable suggestions. X.F. acknowledges the financial support from CHESS under the same NSF award.

■ REFERENCES

(1) Tarascon, J. M.; Armand, M. Issues and Challenges Facing Rechargeable Lithium Batteries. *Nature* **2001**, *414*, 359−367.

(2) Schmuch, R.; Wagner, R.; Hörpel, G.; Placke, T.; Winter, M. Performance and Cost of Materials for Lithium-based Rechargeable Automotive Batteries. *Nat. Energy* **2018**, *3*, 267−278.

(3) Kwade, A.; Haselrieder, W.; Leithoff, R.; Modlinger, A.; Dietrich, F.; Droeder, K. Current Status and Challenges for Automotive Battery Production Technologies. *Nat. Energy* **2018**, *3*, 290−300.

(4) Cabana, J.; Monconduit, L.; Larcher, D.; Palacín, M. R. Beyond Intercalation-based Li-ion Batteries: The State of the Art and Challenges of Electrode Materials Reacting through Conversion Reactions. *Adv. Mater.* **2010**, *22*, E170−E192.

(5) Coughlan, C.; Ibáñez, M.; Dobrozhan, O.; Singh, A.; Cabot, A.; Ryan, K. M. Compound Copper Chalcogenide Nanocrystals. *Chem. Rev.* **2017**, *117*, 5865−6109.

(6) Li, X.; He, X.; Shi, C.; Liu, B.; Zhang, Y.; Wu, S.; Zhu, Z.; Zhao, J. Synthesis of One-Dimensional Copper Sulfide Nanorods as High-Performance Anode in Lithium Ion Batteries. *ChemSusChem* **2014**, *7*, 3328−3333.

(7) Débart, A.; Dupont, L.; Patrice, R.; Tarascon, J. M. Reactivity of Transition Metal (Co, Ni, Cu) Sulphides Versus Lithium: The Intriguing Case of the Copper Sulphide. *Solid State Sci.* **2006**, *8*, 640−651.

(8) Jache, B.; Mogwitz, B.; Klein, F.; Adelhelm, P. Copper Sulfides for Rechargeable Lithium Batteries: Linking Cycling Stability to Electrolyte Composition. *J. Power Sources* **2014**, *247*, 703−711.

(9) McDowell, M. T.; Lu, Z.; Koski, K. J.; Yu, J. H.; Zheng, G.; Cui, Y. In Situ Observation of Divergent Phase Transformations in Individual Sulfide Nanocrystals. *Nano Lett.* **2015**, *15*, 1264−1271.

(10) Han, F.; Li, W.-C.; Li, D.; Lu, A.-H. In Situ Electrochemical Generation of Mesostructured Cu_2S/C Composite for Enhanced Lithium Storage: Mechanism and Material Properties. *ChemElectroChem* **2014**, *1*, 733−740.

(11) Yuan, T.; Tan, Z.; Ma, C.; Yang, J.; Ma, Z.-F.; Zheng, S. Challenges of Spinel $Li_4Ti_5O_{12}$ for Lithium-Ion Battery Industrial Applications. *Adv. Energy Mater.* **2017**, *7*, 1601625−1601625.

(12) Shi, C.; Li, X.; He, X.; Zhao, J. New Insight into the Interaction between Carbonate-based Electrolyte and Cuprous Sulfide Electrode Material for Lithium Ion Batteries. *Electrochim. Acta* **2015**, *174*, 1079−1087.

(13) Meng, X.; Riha, S. C.; Libera, J. A.; Wu, Q.; Wang, H.-H.; Martinson, A. B. F.; Elam, J. W. Tunable Core-shell Single-walled Carbon Nanotube-Cu_2S Networked Nanocomposites as High-performance Cathodes for Lithium-ion Batteries. *J. Power Sources* **2015**, *280*, 621−629.

(14) Kalimuldina, G.; Taniguchi, I. Synthesis and Electrochemical Characterization of Stoichiometric Cu_2S as Cathode Material with

High Rate Capability for Rechargeable Lithium Batteries. *J. Power Sources* **2016**, *331*, 258−266.

(15) Kalimuldina, G.; Taniguchi, I. High Performance Stoichiometric Cu_2S Cathode on Carbon Fiber Current Collector for Lithium Batteries. *Electrochim. Acta* **2017**, *224*, 329−336.

(16) Yu, S.-H.; Feng, X.; Zhang, N.; Seok, J.; Abruña, H. D. Understanding Conversion-Type Electrodes for Lithium Rechargeable Batteries. *Acc. Chem. Res.* **2018**, *51*, 273−281.

(17) Wang, Y.; Zhang, Y.; Li, H.; Peng, Y.; Li, J.; Wang, J.; Hwang, B. J.; Zhao, J. Realizing High Reversible Capacity: 3D Intertwined CNTs Inherently Conductive Network for CuS as an Anode for Lithium Ion Batteries. *Chem. Eng. J.* **2018**, *332*, 49−56.

(18) Ravel, B.; Newville, M. ATHENA, ARTEMIS, HEPHAESTUS: Data Analysis for X-ray Absorption Spectroscopy Using IFEFFIT. *J. Synchrotron Radiat.* **2005**, *12*, 537−541.

(19) Toby, B. H.; Von Dreele, R. B. GSAS-II: the Genesis of a Modern Open-source All Purpose Crystallography Software Package. *J. Appl. Crystallogr.* **2013**, *46*, 544−549.

(20) Carné-Sánchez, A.; Imaz, I.; Cano-Sarabia, M.; Maspoch, D. A Spray-drying Strategy for Synthesis of Nanoscale Metal-organic Frameworks and Their Assembly into Hollow Superstructures. *Nat. Chem.* **2013**, *5*, 203−211.

(21) Li, H.; Wang, Y.; Huang, J.; Zhang, Y.; Zhao, J. Microwave-assisted Synthesis of CuS/Graphene Composite for Enhanced Lithium Storage Properties. *Electrochim. Acta* **2017**, *225*, 443−451.

(22) Hu, H.; Cheng, H.; Liu, Z.; Li, G.; Zhu, Q.; Yu, Y. In Situ Polymerized PAN-Assisted S/C Nanosphere with Enhanced High-Power Performance as Cathode for Lithium/Sulfur Batteries. *Nano Lett.* **2015**, *15*, 5116−5123.

(23) Zhang, Y.; Li, K.; Huang, J.; Wang, Y.; Peng, Y.; Li, H.; Wang, J.; Zhao, J. Preparation of Monodispersed Sulfur Nanoparticles-partly Reduced Graphene Oxide-polydopamine Composite for Superior Performance Lithium-sulfur Battery. *Carbon* **2017**, *114*, 8−14.

(24) Hurma, T.; Kose, S. XRD Raman Analysis and Optical Properties of CuS Nanostructured Film. *Optik* **2016**, *127*, 6000−6006.

(25) He, S.; Wang, G.-S.; Lu, C.; Luo, X.; Wen, B.; Guo, L.; Cao, M.-S. Controllable Fabrication of CuS Hierarchical Nanostructures and Their Optical, Photocatalytic, and Wave Absorption Properties. *ChemPlusChem* **2013**, *78*, 250−258.

(26) Gao, J.; Lowe, M. A.; Kiya, Y.; Abruña, H. D. Effects of Liquid Electrolytes on the Charge−Discharge Performance of Rechargeable Lithium/Sulfur Batteries: Electrochemical and in-Situ X-ray Absorption Spectroscopic Studies. *J. Phys. Chem. C* **2011**, *115*, 25132−25137.

(27) Yim, T.; Park, M.-S.; Yu, J.-S.; Kim, K. J.; Im, K. Y.; Kim, J.-H.; Jeong, G.; Jo, Y. N.; Woo, S.-G.; Kang, K. S.; Lee, I.; Kim, Y.-J. Effect of Chemical Reactivity of Polysulfide Toward Carbonate-based Electrolyte on the Electrochemical Performance of Li−S Batteries. *Electrochim. Acta* **2013**, *107*, 454−460.

(28) Yang, Y.; Zheng, G.; Misra, S.; Nelson, J.; Toney, M. F.; Cui, Y. High-capacity Micrometer-sized Li_2S Particles as Cathode Materials for Advanced Rechargeable Lithium-ion Batteries. *J. Am. Chem. Soc.* **2012**, *134*, 15387−15394.

(29) Wang, X.; Wang, Y.; Li, X.; Liu, B.; Zhao, J. A Facile Synthesis of Copper Sulfides Composite with Lithium-storage Properties. *J. Power Sources* **2015**, *281*, 185−191.

(30) Cheng, J.; Pan, Y.; Zhu, J.; Li, Z.; Pan, J.; Ma, Z. Hybrid Network CuS Monolith Cathode Materials Synthesized via Facile in Situ Melt-diffusion for Li-ion Batteries. *J. Power Sources* **2014**, *257*, 192−197.

(31) Kumar, P.; Nagarajan, R.; Sarangi, R. Quantitative X-ray Absorption and Emission Spectroscopies: Electronic Structure Elucidation of Cu_2S and CuS. *J. Mater. Chem.* **2013**, *1*, 2448−2454.

(32) Wang, Q.; Hanson, J. C.; Frenkel, A. I. Solving the Structure of Reaction Intermediates by Time-resolved Synchrotron X-ray Absorption Spectroscopy. *J. Chem. Phys.* **2008**, *129*, 234502−234507.

(33) Klysubun, W.; Thongkam, Y.; Pongkrapan, S.; Won-in, K.; T-Thienprasert, J.; Dararutana, P. XAS Study on Copper Red in Ancient Glass Beads from Thailand. *Anal. Bioanal. Chem.* **2011**, *399*, 3033−3040.

(34) Greaves, G. N.; Durham, P. J.; Diakun, G.; Quinn, P. Near-edge X-ray Absorption Spectra for Metallic Cu and Mn. *Nature* **1981**, *294*, 139−142.

(35) Rothe, J.; Hormes, J.; Bönnemann, H.; Brijoux, W.; Siepen, K. In Situ X-ray Absorption Spectroscopy Investigation during the Formation of Colloidal Copper. *J. Am. Chem. Soc.* **1998**, *120*, 6019−6023.

(36) Chung, J. S.; Sohn, H. J. Electrochemical Behaviors of CuS as a Cathode Material for Lithium Secondary Batteries. *J. Power Sources* **2002**, *108*, 226−231.

(37) Yamakawa, N.; Jiang, M.; Grey, C. P. Investigation of the Conversion Reaction Mechanisms for Binary Copper (II) Compounds by Solid-State NMR Spectroscopy and X-ray Diffraction. *Chem. Mater.* **2009**, *21*, 3162−3176.

(38) Kalimuldina, G.; Taniguchi, I. Electrochemical Properties of Stoichiometric CuS Coated on Carbon Fiber Paper and Cu Foil Current Collectors as Cathode Material for Lithium batteries. *J. Mater. Chem. A* **2017**, *5*, 6937−6946.

(39) Patel, T. A.; Panda, E. Copper Deficiency Induced Varying Electronic Structure and Optoelectronic Properties of $Cu_{2-x}S$ Thin Films. *Appl. Surf. Sci.* **2019**, *488*, 477−484.

(40) Qiu, P.; Zhu, Y.; Qin, Y.; Shi, X.; Chen, L. Electrical and Thermal Transports of Binary Copper Sulfides Cu_xS with X from 1.8 to 1.96. *APL Mater.* **2016**, *4*, 104805−104805.

(41) You, Y.; Yao, H. R.; Xin, S.; Yin, Y. X.; Zuo, T. T.; Yang, C. P.; Guo, Y. G.; Cui, Y.; Wan, L. J.; Goodenough, J. B. Subzero-Temperature Cathode for a Sodium-Ion Battery. *Adv. Mater.* **2016**, *28*, 7243−7248.

(42) Yuan, Z.; Peng, H. J.; Hou, T. Z.; Huang, J. Q.; Chen, C. M.; Wang, D. W.; Cheng, X. B.; Wei, F.; Zhang, Q. Powering Lithium-Sulfur Battery Performance by Propelling Polysulfide Redox at Sulfiphilic Hosts. *Nano Lett.* **2016**, *16*, 519−527.

(43) Wang, X.; Hao, H.; Liu, J.; Huang, T.; Yu, A. A Novel Method for Preparation of Macroposous Lithium Nickel Manganese Oxygen as Cathode Material for Lithium Ion Batteries. *Electrochim. Acta* **2011**, *56*, 4065−4069.

https://dx.doi.org/10.1021/acsami.9b21982
ACS Appl. Mater. Interfaces 2020, 12, 17396−17405